COMPDYN 2013
4th ECCOMAS Thematic Conference on
Computational Methods in Structural Dynamics and Earthquake Engineering
M. Papadrakakis, V. Papadopoulos, V. Plevris (eds.)
Kos Island, Greece, 12–14 June 2013

APPLCATION OF GENERALIZED PLASTICITY MODEL IN SQUARE CFT COLUMN ANALYSIS

Svetlana M. Kostic[1], Prof. Filip C. Filippou[2], and Prof. Biljana Deretic-Stojanovic[1]

[1] Faculty of Civil Engineering, University of Belgrade
Bulevar Kralja Aleksandra 73, Belgrade, Serbia
e-mail: {svetlana, biljads}@grf.bg.ac.rs

[2] Department of Civil and Env. Engineering, University of California
Berkeley, CA 94720-1710
filippou@ce.berkeley.edu

Keywords: CFT columns, Nonlinear Analysis, Beam-Column Element, Generalized Plasticity, Resultant Plasticity.

Abstract. *In the paper, an efficient three-dimensional concentrated plasticity nonlinear beam-column element is used for the simulation of the response of square CFT columns. The element adopts the concept of the generalized plasticity material model for the section resultant – element deformation relation and has plastic hinges located at the ends of the element and described with yield and limit surfaces. Determination of the adequate element parameters which are essential for a successful description of the CFT member behavior is discussed. Among these parameters, most important are the stiffness and yield surface parameters.*

1 INTRODUCTION

The use of composite concrete-filled steel tubes (CFT), see Figure 1, for the columns of frame structures is in increasing use due to advantages they offer over steel or reinforced concrete members: high stiffness and strength, increased ductility, delayed or prevented buckling, etc. Because of their highly nonlinear behavior, the adequate numerical model needs to address number of phenomena such as: nonlinear steel and concrete material behavior, buckling of steel tube and sleep at the steel-concrete interface.

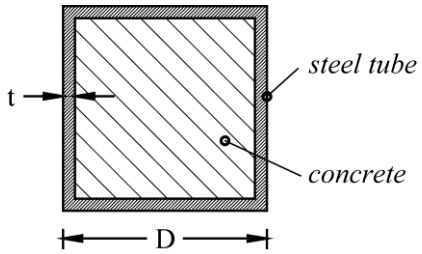

Figure 1: Square concrete filled tube (CFT).

To date, although a number of experimental studies have been performed on behavior of CFT columns [1], not many analytical models have been developed. Few researchers studied the ultimate strength of a composite cross-section under biaxial bending in presence of axial force [2, 3]. Besides continuum finite element models [4] which may be appropriate for detailed analysis of a part of a structure (e.g. joints), frame beam/column elements are still primarily used for the CFT member and composite frame analysis. Hajjar and Gourley [5, 6] developed a concentrated plasticity 3D finite element for the simulation of a CFT beam-column behavior. The plastic hinges at the element ends are described by a two-surface, bounding surface model in the stress-resultant P-M_y-M_z space. Iu, Bradford and Chen [3] developed a concentrated plasticity element with axial and rotational springs at element ends suitable for modeling composite beam-column members. It describes non-linear elastic-plastic with strain-hardening material behavior with gradual transition between elastic and plastic domain, under the interaction of axial force and two bending moments. More accurate, but also computationally more involving are distributed plasticity elements. Fiber-based distributed plasticity elements have proven to be successful in simulation of the hysteretic response of steel, concrete and composite structures [7-9]. For modeling of CFT columns, few proposals have been made [1, 8, 10]. They also account for geometrical nonlinearities and an interlayer sleep at the steel-concrete interface.

The purpose of this study is to show that the previously developed non-linear beam-column element [11] used for static and dynamic analysis of steel frames, with the proper choice of element parameters, can also be successfully used for modeling CFT column behavior. The element is of concentrated plasticity type and based on the principles of generalized plasticity material model [12]. It accounts for the interaction of the axial force and bending moments about the principal axes of the cross-section, gradual yielding of the cross section and the hardening behavior. With the implemented return mapping algorithm, it is computationally very efficient.

2 BASICS OF ELEMENT FORMULATION

More details about the element used in this study, named GP element, can be found in [11]. Here will be given only the basics of the element formulation. The element is of concentrated plasticity type and has two zero-length plastic hinges at element ends (Figure 2). It adopts

concept of the generalized plasticity material model [12] for the section resultant (forces) – element deformation relations. The plastic hinges are described by the yield function *f*, which encloses the elastic region, and the limit function *F*, which separates admissible from inadmissible stress-resultant states (see Figure 2). The basic forces of a three-dimensional frame element are **q**, and the corresponding deformations are denoted with **v** as shown in Figure 3 for the 3D case. Torsion is considered as elastic and uncoupled from the axial and flexural degrees of freedom and, thus, not shown in Figure 3.

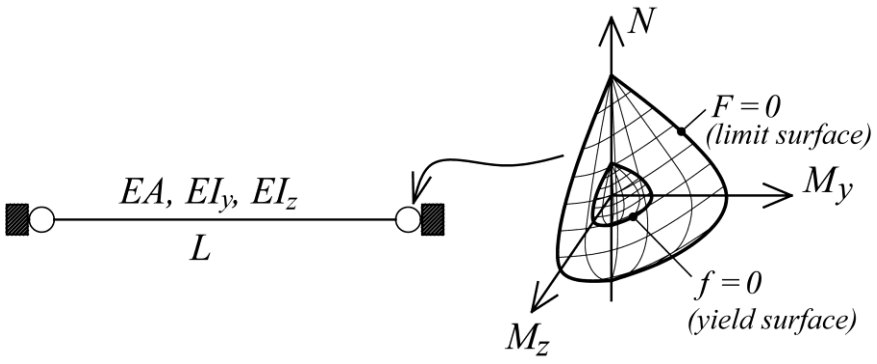

Figure 2: Element end plastic hinges with yield and limit surfaces.

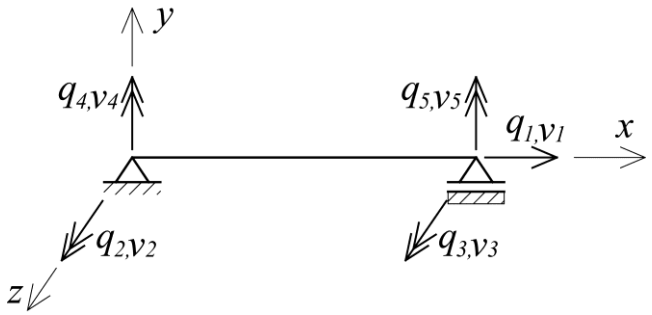

Figure 3: Basic element forces **q** and corresponding deformations **v**.

The basic element equations are:

1. The element deformations **v** are decomposed into the linear elastic, and the plastic contribution, i.e. $\mathbf{v^e}$ and $\mathbf{v^p}$:

$$\mathbf{v} = \mathbf{v^e} + \mathbf{v^p} \tag{1}$$

2. The relation between the basic element forces **q** and the elastic element deformations $\mathbf{v^e}$ is assumed to be linear:

$$\mathbf{q} = \mathbf{k_e}\mathbf{v^e} = \mathbf{k_e}\left(\mathbf{v} - \mathbf{v^p}\right) \tag{2}$$

where $\mathbf{k_e}$ is the elastic stiffness matrix.

3. The yield function *f* at each element end is assumed in the following form:

$$f(\mathbf{q}, \mathbf{a}, \alpha) = \Phi(\mathbf{q} - \mathbf{a}) - H_{iso}\alpha \tag{3}$$

A vector **a** describes the position of the center of the yield surface and its evolution determines the kinematic hardening mechanism. A variable α is a hardening variable which represents the isotropic hardening. More details about the adopted form of evolution laws for **a** and α can be found in [11]. H_{iso} is the non-dimensional isotropic hardening parameter.

4. The adopted limit function F has the following form (as proposed in the generalized plasticity models [12]):

$$F = h(f)\frac{d}{dt}(\Phi) - \lambda \tag{4}$$

$$h(f) = \frac{f}{\delta(\beta - f) + (H_{iso} + H_{kin})\beta} \tag{5}$$

H_{kin} is the non-dimensional kinematic hardening parameter, and δ and β are two positive non-dimensional constants. δ measures the rate of approaching the asymptotic behavior, and β is a measure of the distance between the yield function f and the asymptote, as shown in Figure 4. Parameter λ is the nonnegative consistency parameter.

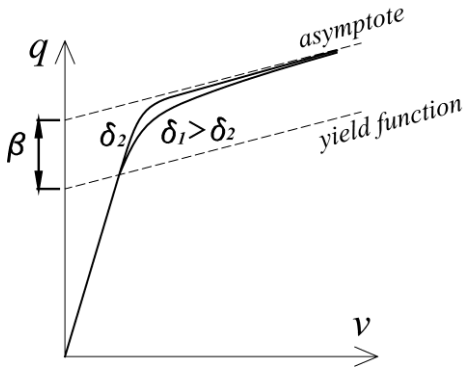

Figure 4: Meaning of parameters δ and β.

5. The flow rule is assumed as associative with the evolution relation:

$$\dot{\mathbf{v}}^{\mathbf{p}} = \lambda \frac{\partial f}{\partial \mathbf{q}} \tag{6}$$

As explained in [11], the proposed model, by applying the backward Euler algorithm, can be successfully transferred into a discrete problem that can be efficiently numerically solved by the two step elastic predictor – plastic corrector return mapping algorithm [13].

3 CHOICE OF ELEMENT PARAMETERS

The GP element was successfully applied for the analysis of steel beam/column and frame behavior. The aim of this study is to show that the element can also be successfully used for modeling the CFT column behavior, but with the proper choice of element parameters.

Considering behavior of CFT columns, the following assumptions are adopted. CFT sections are completely filled with concrete and without shear connectors at the steel concrete interface. The perfect bond between steel and concrete is assumed, without any sleep, which is an often assumption in analytical studies [2]. Viscous deformations of concrete, creep and shrinkage, have been neglected since it has been shown to have little influence on the CFT column behavior. Also, the flexural-torsional and the lateral-torsional buckling are neglected. Residual stresses present in the steel tube and the local buckling of the steel tube are taken into account indirectly, by the yield surface parameters [5].

The essential for a successful description of a CFT member behavior is the determination of the GP element parameters. The expressions and values adopted in this study for each of them are discussed in the following.

3.1 Stiffness of a CFT section

Since a CFT cross-section is made of two different materials, steel and concrete, stiffness of a composite section is determined as follows:

- The axial stiffness is taken as a summation of the axial stiffness of each part of a CFT section, i.e. $(EA)_{CFT} = E_s \cdot A_s + E_c \cdot A_c$, where E_s and E_c are moduli of elasticity of steel and concrete. A_s and A_c are areas of steel and concrete part of a composite section.
- The bending stiffness is taken as a summation of the bending stiffness of the steel part of a CFT section and the reduced stiffness of the concrete part of a composite section (due to the concrete cracking effects), i.e. $(EI)_{CFT} = E_s \cdot I_s + \beta \cdot E_c \cdot I_c$, where I_s and I_c are the moments of inertia of steel and concrete part of a composite section. To date, a number of proposals for the reduction coefficient β have been made [14]. However, the comparison made during this study has shown that a constant value of $\beta=0.6$ proposed by Eurocode 4 [15] ensures, for practical application, enough accurate results.
- The torsional stiffness is determined as the torsional stiffness of the steel part of a CFT section, i.e. $(GI_t)_{CFT} = G_s \cdot I_{t,s}$, where G_s is the shear modulus of steel, and $I_{t,s}$ is a torsion constant of the steel part of a CFT section. This approximation is acceptable in cases with small torsional effects.

3.2 Yield surface parameters for a CFT section

The yield surface equation in the N-M_z-M_y stress resultant space is adopted in the form proposed by Hajjar and Gourley [2] for analysis of a rectangular CFT section:

$$\begin{aligned} &f(p, m_z, m_y) = \\ &c_1 \cdot (m_y^2 + m_z^2) + c_2 \cdot p^2 + c_3 \cdot (m_y^2 \cdot p^2 + m_z^2 \cdot p^2) + c_4 \cdot m_y^2 \cdot m_z^2 - c \end{aligned} \tag{7}$$

Coefficients c_1, c_2, c_3 and c_4 are obtained by calibration with a fiber section and depend on the ratio between height and depth of steel section (D/t), and the ratio between the concrete compressive strength and the yield stress of steel (f_c'/f_y). The exact expressions for these coefficients can be found in [2]. The arguments p, m_z and m_y in the expression (7) are defined as:

$$p = \frac{P - \varphi \cdot P_0}{P_0}, \quad m_z = \frac{M_z}{M_{z0}}, \quad m_y = \frac{M_y}{M_{y0}} \tag{8}$$

where M_{z0} and M_{y0} are the bending moment ultimate strengths for the CFT section about the z and y axes, determined from the fully plastified section in the absence of axial force $(N=0)$, with the area of concrete in compression taken into account with full amount and the reduced area of concrete in tension, taken with the reduction factor 0.5. Concrete tension strength is taken as $f_t = 0.623\sqrt{f_c'}$ (in MPa) [2]. The value φ defines the eccentric position of the yield surface as Figure 5 shows and, here, it is taken as equal to

$$\varphi = \frac{0.5 \cdot (A_c \cdot f_c' - A_c \cdot f_t)}{P_0} \tag{9}$$

and P_0 is the axial compressive capacity of a CFT section. The parameter c in the expression (7) determines the size of the yield surface. Here, for monotonic loading, it is taken equal to the square of the radius of the initial loading surface proposed by Hajjar and Gourley [2]:

$$c = R_{LS,initial}{}^2 = \left(\frac{M_{yld}}{M_0} - 0.3 \cdot \frac{P_{c0}}{P_0} \right)^2 \tag{10}$$

In this expression, M_{yld} is the plastic moment capacity of a steel section; P_{c0} is the axial compressive capacity of the concrete part of a composite section, i.e. $P_{c0} = A_c \cdot f_c^{'}$.

Under cyclic loading, the elastic zone decreases (the yield surface shrinks). Therefore, a better response of the GP model may be obtained if a lower value for the parameter c is adopted. The authors' recommendation is to use the following value under the cyclic loading conditions:

$$c = \left(\frac{R_{LS,initial} + R_{LS,final}}{2} \right)^2 \tag{11}$$

which has shown to be an adequate approximation. In the last expression, $R_{LS,final}=0.1$ is the final radius of the elastic zone proposed by Hajjar and Gourley [6]. The effect of this parameter c on a column response is demonstrated in one of the following examples.

The parameter β of the GP model is determined as the difference $\beta = (1.0 - c)$.

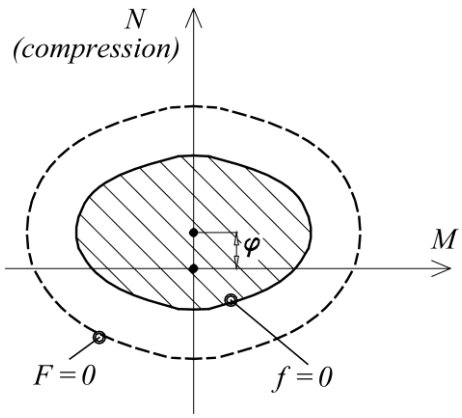

Figure 5: Eccentric position of yield surface (2D case).

3.3 Hardening parameters

The following two features are also important for the adequate simulation of a CFT column behavior.

- The Bauschinger effect is, principally, the result of the steel tube behavior [5]. It can be expressed by the kinematic hardening. In the GP element, it is specified through the H_{kin} parameter.
- Under the cyclic loading conditions, the strength of CFT columns decreases due to the concrete cracking and the local buckling of a steel tube [5]. As a consequence, the limit surface decreases. In the GP element, this effect is approximated with the isotropic hardening (softening) mechanism and a small negative value for the H_{iso} parameter.

4 NUMERICAL EXAMPLES

With the previously adopted element parameters, the capabilities of the GP element to simulate the behavior of composite CFT columns are verified through the following three examples. The response of the GP element is compared with the experimental results available in the literature. FEDEASLab, a Matlab toolbox for nonlinear static and dynamic analysis [16], is used for the simulation.

4.1 Simple beam tests

The first group of tests refers to the tests by Tomii and Sakino [17] on the simple beam exposed to constant axial compressive force and monotonically increasing end moments (Figure 6). Tests number II-2, II-3, II-5, II-6, IV-3 and IV-5 are performed. Details about the beam cross-section, loading and material parameters are given in Table 1. In these tests, steel hardening was about 1%, and in the GP model, it was counted with the kinematic hardening parameter $H_{kin}=0.006$. Results of the GP model are shown in Figure 7 with the full blue line. Experimental results, taken from [6], are presented with black dots.

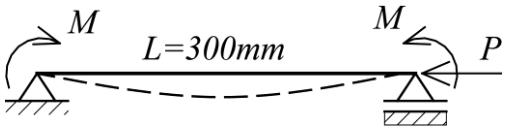

Figure 6: Simple beam and loading [17].

Test	Dimensions (mm)	fc' (MPa)	f_y (MPa)	P/P_0
II-2	100x100x2.27	25.9	339.0	0.18
II-3	100x100x2.20	25.9	339.0	0.26
II-5	100x100x2.22	25.9	289.0	0.48
II-6	100x100x2.22	25.9	289.0	0.57
IV-3	100x100x4.25	22.4	288.0	0.29
IV-5	100x100x4.25	23.8	285.0	0.48

Table 1: Details of CFT simple beam tests [17].

As can be seen from these results, there is a good correlation between the numerically obtained results with the GP model and experimental results considering the initial stiffness and also the limit value of bending moments for all levels of axial force.

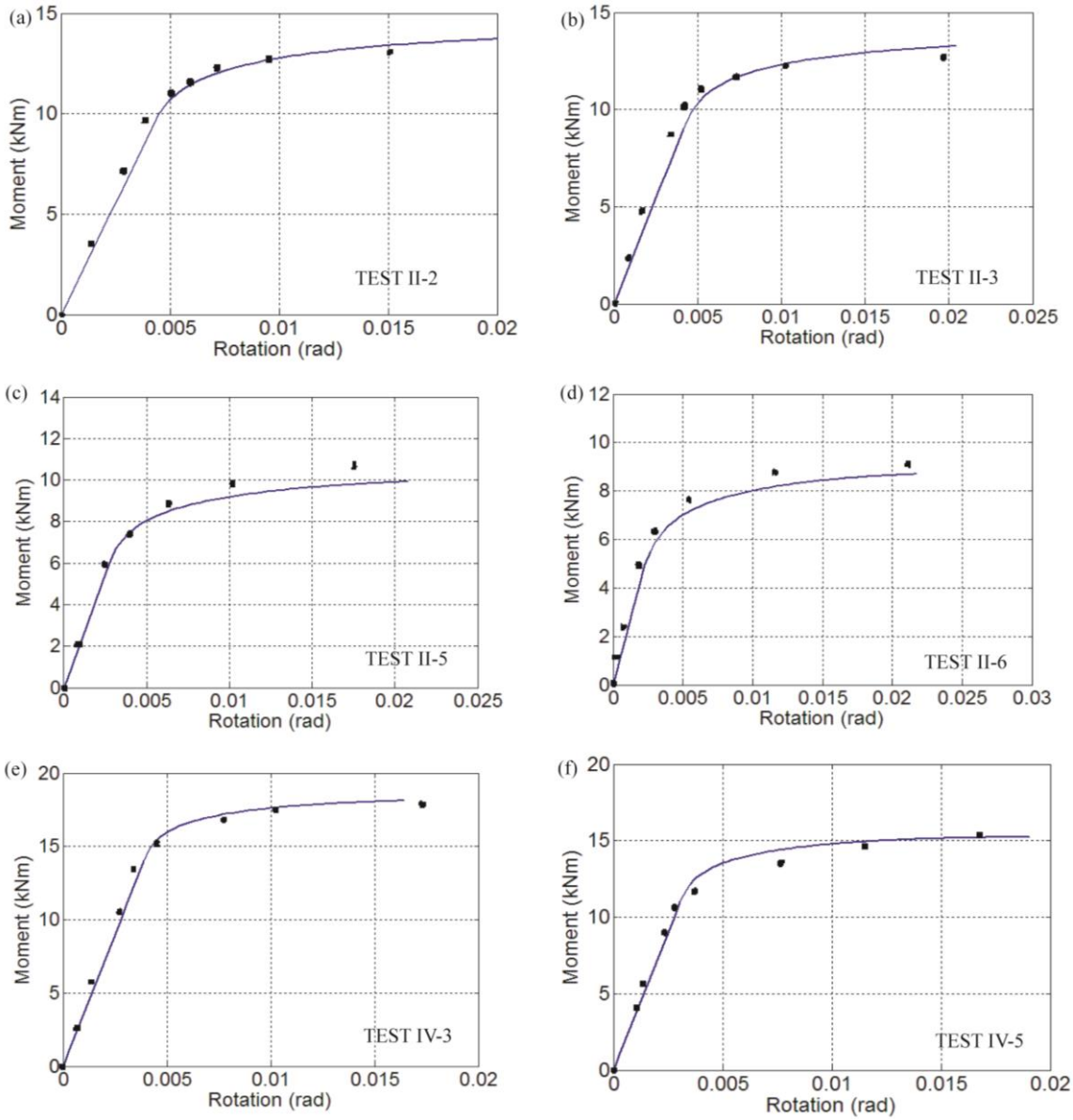

Figure 7: Comparison of experimental and numerical results of moment – rotation relation for Tomii and Sakino [17] tests number II-2, II-3, II-5, II-6, IV-3, IV-5 .

4.2 Beam-column joint

The next example is the 3D analysis of an interior beam-column joint experimentally studied by Kawaguchi and Morino [18]. The joint consists of a square CFT column and three wide flange steel beams, as shown in Figure 8. In this study, the test number I-15C20 is numerically simulated with the use of the GP element.

The joint is firstly loaded with the constant compressive force $P=0.15P_0$ acting on the top of the column, and with the constant axial force $W=21kN$ acting on the free ends of the beam in the *y*-*z* plane, to simulate gravity loading. The earthquake loading is simulated with the asymmetrical loading Q acting on the free ends of the beams in the *x*-*z* plane. The forces Q increase until reaching the following values for rotations R: *0.005*, *0.01*, *0.02* and *0.03*. For each value R, two full cycles are performed. The rotation R is determined from the displacements of points A and B, i.e. the vertical displacements D_1 and D_2 in Figure 9(a). The rotation R is then calculated from the expression:

$$R = \frac{D_1 + D_2}{L} \tag{12}$$

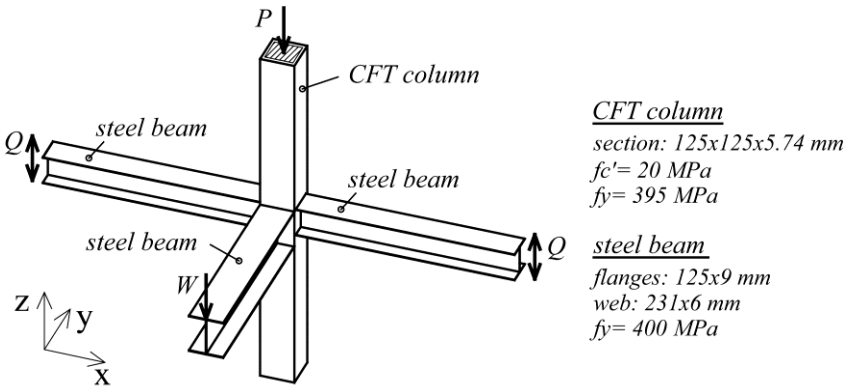

Figure 8: 3D model of interior frame joint and members data.

Figures 9(a) and 9(b) show the numerical model with boundary conditions and the used finite element mesh. It should be noted that, in the example, dimensions of the column and the beams are determined in a way that the joint capacity is governed by the capacity of the CFT column, while beams stay inside the elastic domain during the experiment. Therefore, modeling of beams is irrelevant and instead of the GP, simple linear-elastic elements could be used. In the test, steel tube hardening is 1%, and, in the GP model, it is counted with the kinematic hardening parameter $H_{kin}=0.06$. The slight shrinkage of the limit surface is approximated with the isotropic hardening parameter $H_{iso}=-0.05$.

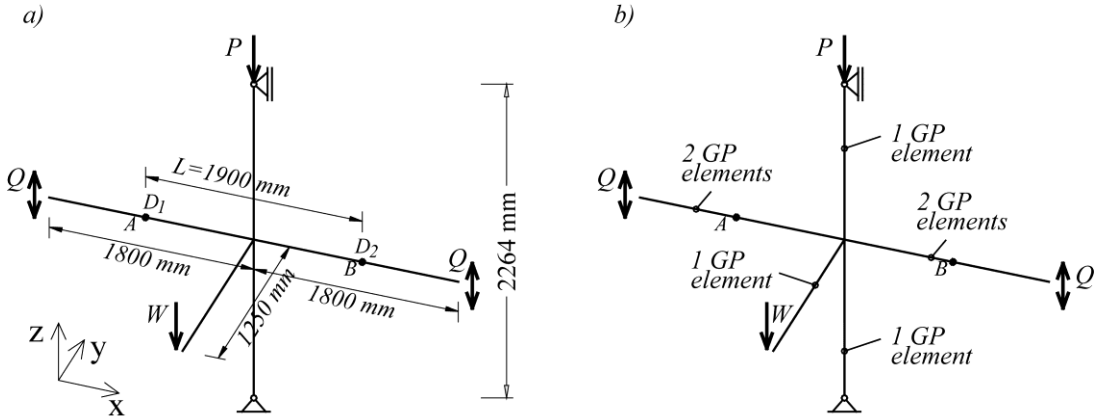

Figure 9: (a) Numerical model and dimensions; (b) Finite element mesh.

The comparison for the *Q*-*R* relation between the experimental results in Figure 10(a), taken from [18], and the numerical results in Figure 10(b) with the GP element and the parameter $c=(R_{LS,initial})^2$ suitable for monotonic loading, shows that the GP model represents well the whole hysteresis curve. The CFT column is exposed to the cyclic biaxial bending with the axial compressive force. As in the previous example, the initial stiffness and the ultimate strength are determined with a high precision. However, as mentioned before, since the elastic zone decreases under the cyclic loading conditions, as a consequence, the limit value for *Q* is approaching at a slower rate. Therefore, a better response of the GP model may be obtained with the proposed value for *c* (expression (11)) which is suitable for cyclic loading. Figure 11 shows results with this value *c*.

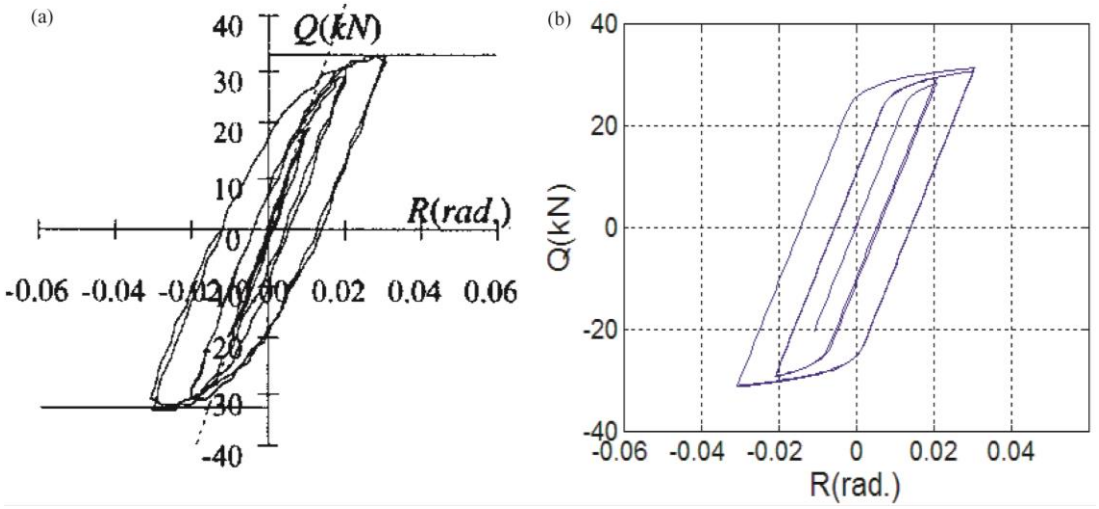

Figure 10: Q-R relation for Kawaguchi and Morino [18] beam-column joint: (a) experimental results; (b) numerical results with GP element and *c* determined from expression (10).

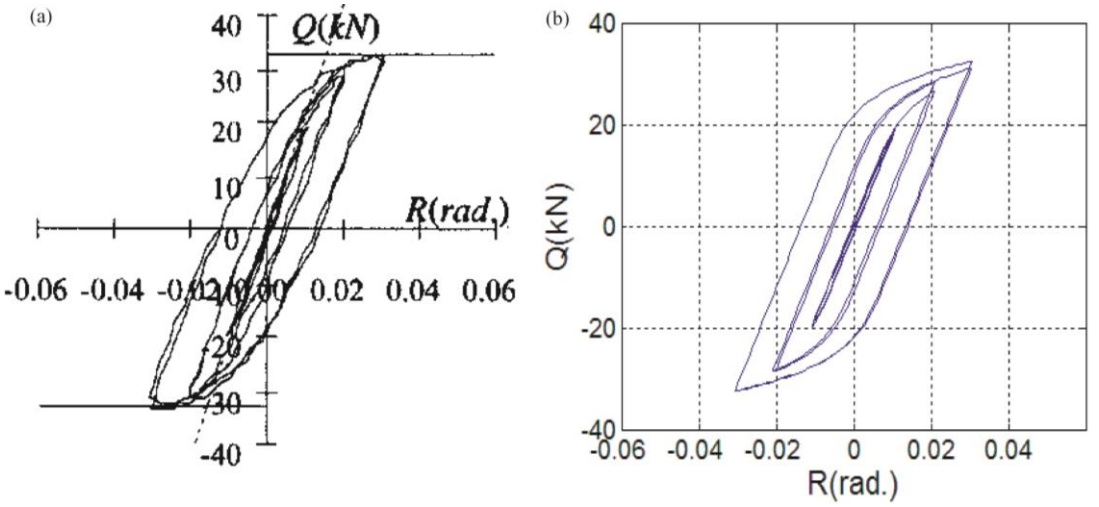

Figure 11: Q-R relation for Kawaguchi and Morino [18] beam-column joint: (a) experimental results; (b) numerical results with GP element and *c* determined from expression (11).

4.3 Portal frame

The last example is the portal frame in Figure 12, experimentally studied by Kawaguchi et al. [19]. The frame consists of two square CFT columns and a steel H-shaped beam. Gravity load is applied first and kept constant, while the frame is subjected to the cyclic lateral loading through the imposed lateral displacements. The loading history in Figure 13 shows the history of the column chord rotation angle R ($R=d/h$). The test number 21SCC30 is numerically simulated with the model with GP elements. In this test, the beam is designed to behave elastically until the end of the test, while the CFT columns yield. The nonlinear geometry under large displacements is accounted for with the corotational formulation [20]. The steel tube hardening is 1%, and the hardening parameters of the GP element are the same as in the previous example.

Figure 14 shows the results of the experiment, taken from [19], and the numerical simulation for the relation between the horizontal force H and the column chord rotation R. As can be seen, generally, the GP model represents well the experimental behavior. The ultimate

strength and the initial stiffness are determined quite accurately. The obtained hysteresis loop is less accurate because of faster (shallower) gradual stiffness reduction of the CFT column than in the GP model. This is also, somewhat, present in the previous example, in Figure 11. It is expected that better representation of this effect will be obtained if the damage mechanics parameters are included into the GP element formulation. However, despite of this fact, the results of the GP model are of acceptable accuracy in general.

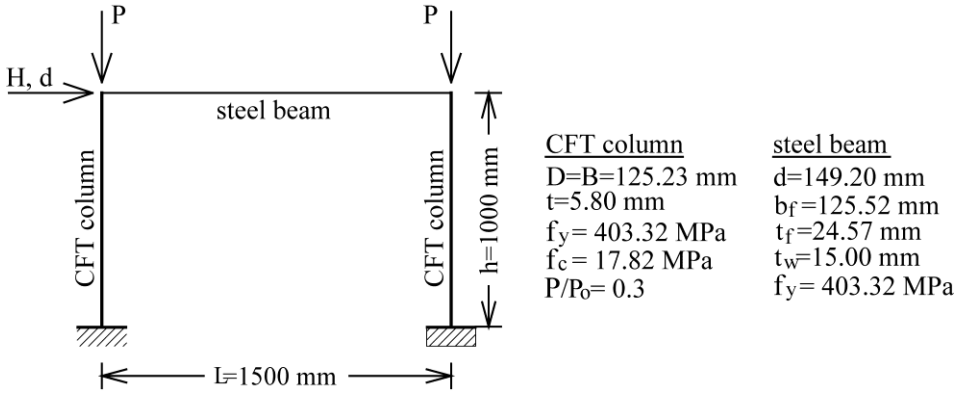

Figure 12: Portal frame [19].

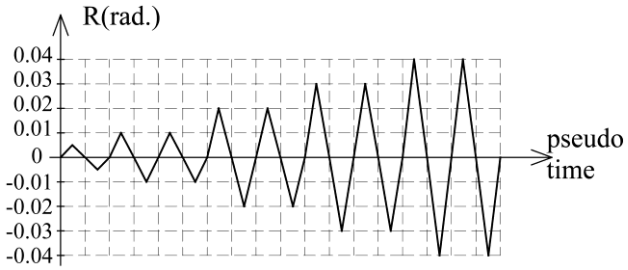

Figure 13: Column chord rotation loading history.

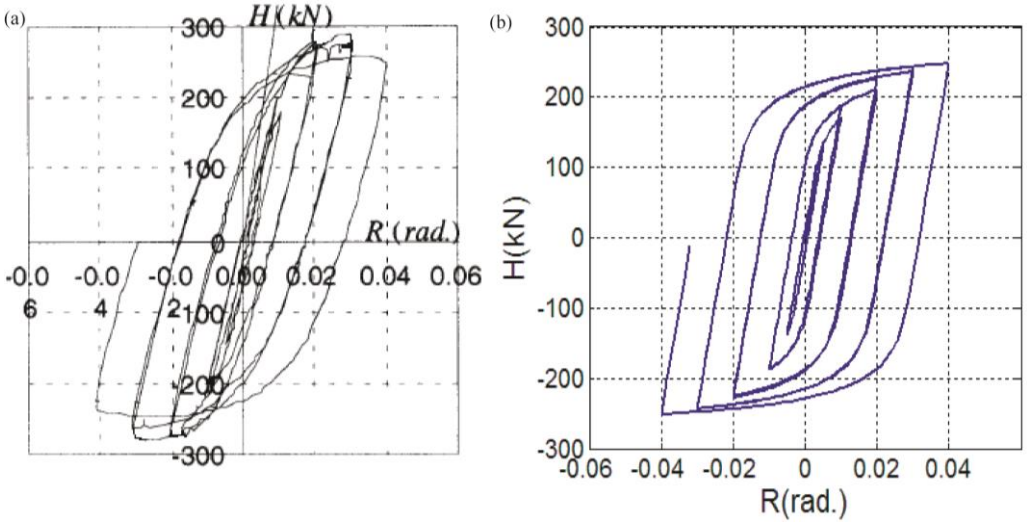

Figure 14: H-R relation for Kawaguchi et al. portal frame [19]: (a) experimental results; (b) numerical results with the GP element.

5 CONCLUSIONS

In the paper, the three-dimensional nonlinear beam-column element, named GP element, is used for the simulation of the response of square CFT columns under monotonic and cyclic loading conditions. The CFT column behaves highly nonlinearly due to number of different effects, i.e. nonlinear steel and concrete material behavior, buckling of steel tube, sleep at the steel-concrete interface, etc. The GP element is of concentrated plasticity type with plastic hinges at element ends and adopts the concept of the generalized plasticity material model for the section resultant – element deformation. It accounts for the interaction of the axial force and bending moments about the principal axes of the cross-section, gradual yielding of the cross section and the hardening behavior. In order to capture some of the most characteristic features of the CFT column behavior, determination of adequate element parameters is discussed in the paper: the loading and the limit surface, the element stiffness and the hardening parameters.

The capability of the GP element in simulation of the CFT column behavior is verified with the three examples where its response is compared with the experimental data. The results showed the high level of accuracy of the element response under monotonic loading conditions, and good accuracy under cyclic loading conditions. With the implemented return mapping algorithm and its high computational efficiency, it may be a good choice for practical applications.

ACKNOWLEDGE

The first author thanks the Ministry of Science of the Republic of Serbia for financial support under project TR 36046.

REFERENCES

[1] A. H. Varma, *et al.*, "Seismic behavior and modeling of high-strength composite concrete-filled steel tube (CFT) beam–columns," *Journal of Constructional Steel Research*, vol. 58, pp. 725-758, 2002.

[2] J. F. Hajjar and B. C. Gourley, "Representation of concrete-filled steel tube cross-section strength," *Journal of Structural Engineering*, vol. 122, p. 1327, 1996.

[3] C. K. Iu, *et al.*, "Second-order inelastic analysis of composite framed structures based on the refined plastic hinge method," *Engineering Structures*, vol. 31, pp. 799-813, 2009.

[4] H.-T. Hu, *et al.*, "Finite element analysis of CFT columns subjected to an axial compressive force and bending moment in combination," *Journal of Constructional Steel Research*, vol. 61, pp. 1692-1712, 2005.

[5] J. F. Hajjar and B. C. Gourley, "A cyclic nonlinear model for concrete-filled tubes. I: Formulation," *Journal of Structural Engineering*, vol. 123, p. 736, 1997.

[6] J. F. Hajjar and B. C. Gourley, "A cyclic nonlinear model for concrete-filled tubes. II: Verification," *Journal of Structural Engineering*, vol. 123, p. 745, 1997.

[7] E. Spacone, *et al.*, "Fiber Beam-Column Model for Nonlinear Analysis of RC Frames: II: Applications," *Earthquake Engineering and Structural Dynamics*, vol. 25, pp. 727-742, 1996.

[8] J. F. Hajjar, *et al.*, "A distributed plasticity model for cyclic analysis of concrete-filled steel tube beam-columns and composite frames," *Engineering Structures*, vol. 20, pp. 398-412, 1998.

[9] R. M. de Souza, "Force-Based Finite Element for Large Displacement Inelastic Analysis of Frames," Ph.D., Civil and Environmental Engineering, University of California, Berkeley, 2000.
[10] C. Tort and J. F. Hajjar, "Mixed Finite-Element Modeling of Rectangular Concrete-Filled Steel Tube Members and Frames under Static and Dynamic Loads," *Journal of Structural Engineering*, vol. 136, pp. 654-664, 2010.
[11] S. M. Kostic, *et al.*, "An Efficient Beam-Column Element for Inelastic 3D Frame Analysis," in *Computational Methods in Earthquake Engineering*. vol. 2, M. Papadrakakis, *et al.*, Eds., ed: Springer, 2013, p. to be published.
[12] J. Lubliner, *et al.*, "A New Model of Generalized Plasticity and Its Numerical Implementation," *International Journal of Solids and Structures*, vol. 30, pp. 3171-3184, 1993.
[13] J. C. Simo and T. J. Hughes, *Computational Inelasticity*. Secaucus, NJ, USA: Springer-Verlag New York, Incorporated, 1998.
[14] J. Moon, *et al.*, "Analytical modeling of bending of circular concrete-filled steel tubes," *Engineering Structures*, vol. 42, pp. 349-361, 2012.
[15] E. C. f. Standardization, "Design of Composite Steel and Concrete Structures - Part 1.1: General Rules and Rules for Buildings, Eurocode 4," ed. Brussels: European Comitee for Standardization, 2004.
[16] F. C. Filippou and M. Constantinides, "FEDEASLab Getting Started Guide and Simulation Examples," University of California, Berkeley, Technical Report2004.
[17] M. Tomii and K. Sakino, "Experimental Studies on the Ultimate Moment of Concrete Filled Square Steel Tubular Beam-Columns," *Trans. Arch. Inst. of Japan*, pp. 55-63, January 1979.
[18] J. Kawaguchi and S. Morino, "Experimental Study on Post-Local Buckling Behavior of CFT Beam-Columns Under Cyclic Loading, Elasto-Plastic Behavior of Square CFT Beam-Columns: Part 1," *J. Struct. Constr. Eng., Architectural Inctitute of Japan*, pp. 141-148, February 2001.
[19] J. Kawaguchi, *et al.*, "Structural Behavior and Characteristics of Concrete-Filled Tubular Frames," Faculty of Engineering, Mie University, Research report1997.
[20] M. A. Crisfield, *Non-linear finite element analysis of solids and structures*. West Sussex: John Wiley & Sons, 1991.